Stabilizing Monomeric Iron Species in a Porous Silica/Mo(112) Film

Jan-Frederik Jerratsch,[†] Niklas Nilius,[†,]* Dinesh Topwal,[‡] Umberto Martinez,[§] Livia Giordano,[§] Gianfranco Pacchioni,[§] and Hans-Joachim Freund[†]

[†]Department of Chemical Physics, Fritz-Haber-Institute, Faradayweg 4-6, D-14195 Berlin, Germany, [‡]International Center for Theoretical Physics, Strada Costiera 11, 34100 Trieste, Italy, and [§]Dipartimento di Scienza dei Materiali, Università di Milano-Bicocca, via Cozzi, 53-20125 Milano, Italy

ABSTRACT The stabilization of single Fe atoms in the nanopores of an ultrathin silica film grown on Mo(112) is demonstrated with scanning tunneling microscopy (STM) and density functional theory (DFT). The Fe atoms are able to penetrate the openings in the oxide surface and adsorb in two different binding configurations at the metal—oxide interface. In the energetically preferred site, the Fe stays monomeric even at temperatures above 300 K. In the second configuration that is adopted in 10% of the cases, surface atoms can be attached to the subsurface species, resulting in the formation of Fe surface clusters. The interfacial Fe atoms preserve their magnetic moment, as shown by a distinct Kondo-like response in STM conductance spectra and DFT calculations.

KEYWORDS: single Fe atoms · porous silica film · magnetic properties · Kondo effect · scanning tunneling microscopy · density functional theory

The storage capacity of magnetic hard drives has exponentially increased over the last several years. This immense progress was achieved due to new read-out technologies based on the giant magneto-resistance effect.[1] Additionally, the magnetic region that represents one bit has continuously decreased. In the present state-of-the-art technology, one magnetic bit comprises an area of roughly 10^3 to 10^4 nm^2 in a Co—Cr—Pt alloy film. In the next steps of miniaturization, the continuous magnetic films will be replaced by an ordered array of Fe, Co, or Ni clusters with superparamagnetic properties, fabricated *via* wet-chemical synthesis or buffer-layer-assisted growth.[2−4] In the ultimate limit of down-scaling, a single adatom or molecule may represent one magnetic unit. The information will then be retained in the orientation of a single magnetic moment and not in the collective magnetization of hundreds of atoms. Experiments along this line have been accomplished for single magnetic adatoms (*e.g.*, Co and Mn)[5−7] and molecules (*e.g.*, CoPc and FePc),[8,9] employing magnetic dichroism and scanning tunneling microscopy (STM). However, fundamental problems in the use of magnetic atoms and molecules are not yet solved. The magnetic buildings blocks need to be arranged in regular arrays and stabilized against diffusion and aggregation at room temperature. Furthermore, the interaction of an isolated moment with its environment has to be balanced in a way that controlled switching of the spin direction is possible while unwanted thermal fluctuations are suppressed. Only if these structural and magnetic requirements are fulfilled, single adatoms and molecules

might become the key elements in the next generation of storage devices.

In this paper, we focus on the structural side of the problem and introduce a new approach that enables the stabilization of single magnetic atoms in near-surface sites even at elevated temperatures. An ultrathin silica/Mo(112) film that can be considered as a 2D counterpart of a porous silicate is used as a template.[10] The oxide film comprises a single layer of corner-sharing SiO_4 tetrahedrons, whereby three O atoms bind to neighboring Si atoms in the plane, while the fourth one sits below the Si and anchors the film to the support. The in-plane —Si—O— units form six-membered rings of 5 Å diameter, which enclose a hole reaching down to the Mo surface. As shown in earlier experiments, those oxide nanopores can be loaded with suitable metal atoms, such as Li, Ag, and Pd, whereas Au atoms are too large for penetration.[11,12] Incorporation of metal atoms has been used to tailor the intrinsic properties and the adsorption behavior of the oxide material, for instance, by creating chemically selective binding sites in the surface.[13,14] In this study, we exploit the porous structure of the silica film to produce a thermally stable ensemble of
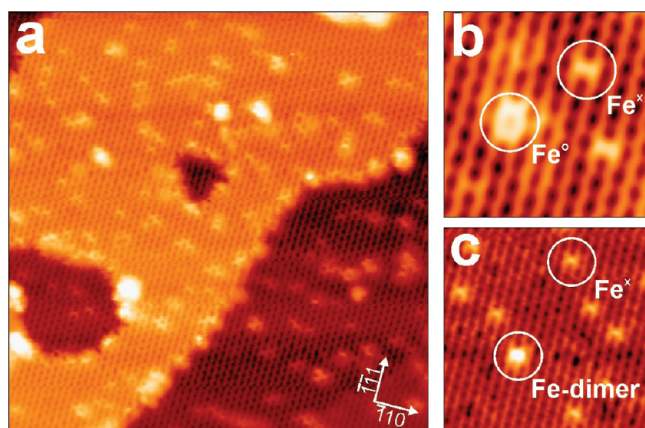
Figure 1. (a) STM image of silica/Mo(112) after deposition of 0.04 Fe atoms per silica pore (U_s = 0.6 V, 40 × 40 nm²). (b) Close-up STM image (U_s = 0.5 V, 5 × 5 nm²) with subsurface Fe° and Fe^x species marked by white circles. (c) STM image (U_s = 0.5 V, 10 × 10 nm²) showing an Fe dimer as well as a few monomeric species.

Fe monomers. The incorporation of Fe into the oxide matrix has a number of advantages with respect to conventional atom deposition onto flat surfaces. (i) The Fe is stabilized against diffusion and desorption even at elevated temperature, as leaving the pore is associated with a substantial energy barrier.[12,15] (ii) The aggregation of the Fe is prevented by the limited pore size that provides only space for a single atom. (iii) The iron is protected against environmental influences, as the silica surface is chemically inert and does not interact with molecules from the gas phase.[16] Incorporation of Fe into the silica/Mo(112) film is therefore a promising route to fabricate a dense ensemble of monomeric magnetic entities for potential storage applications. The unique properties of the Fe–silica system are disclosed in this study by employing low-temperature STM and density functional theory (DFT).

RESULTS AND DISCUSSION

Fe Monomers: Structural Properties. Figure 1a shows an overview STM image of the silica/Mo(112) film after deposition of 1.5 × 10¹³ Fe atoms/cm² or correspondingly 0.04 atoms per silica pore. Two oxide terraces are exposed, both being fully covered by the hexagonal hole pattern that is characteristic for the porous film structure. The uniform film appearance is disrupted by

a number of faint, randomly distributed protrusions, which are assigned to the Fe species. Occasionally, larger maxima with 1–4 Å height are observed that might represent small Fe clusters. Close-up STM images enable an atomic-scale characterization of the different Fe species (Figure 1b). The most frequently observed feature is an X-shaped protrusion, which is located at the intersection of two six-membered silica rings and oriented along the Mo[$\bar{1}$10] direction (referred to as Fe^x). Its apparent height shows a characteristic bias dependence and increases from 0.3 Å at 0.1 V sample bias to a maximum of 0.8 Å at 2.5 V (Figure 2). Additionally, ring-like protrusions (Fe°) are detected that appear slightly brighter than the X-shaped features in the explored bias window. They coincide with the size and shape of a single –Si–O– ring in the silica film. The density of the ring-like protrusions is roughly 10 times lower than that of the Fe^x species. With increasing Fe exposure, larger adstructures develop on the surface. The smallest of them still has atomic dimensions and occupies the same adsorption sites as the Fe° species. Its apparent height is two times larger than that of the Fe^x features and increases from 0.5 Å at low bias to 1.5 Å at 2.5 V (Figure 2b). Furthermore, a few Fe clusters emerge on the surface and quickly grow in size with increasing metal exposure.

The experimentally observed adspecies can be assigned to distinct Fe adsorption configurations with the help of DFT calculations. The Fe atoms are predicted to pass the six-membered –Si–O– rings in the silica surface and reach high-energy binding sites at the metal–oxide interface. The calculated penetration barrier amounts to 0.3 eV, a value that is easily overcome by the thermal Fe atoms arriving with ~0.1 eV from the crucible. Similar penetration barriers have been calculated for Ag and Li atoms, which also reach interfacial binding sites of the silica/Mo system.[12,17] The origin of the penetration barrier is rather different for the three atoms. While Li penetrates as a cation and forms bonds with the silica O atoms upon passage, Fe and Ag atoms diffuse into the pores as neutral species. In this case, the barrier is governed by repulsive interactions between the charge density at the oxide surface and electrons in the valence orbitals of Fe and Ag. Two
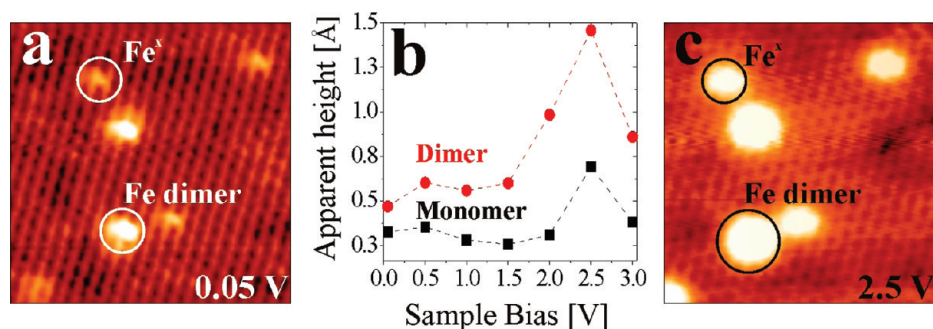

Figure 2. (a,c) STM images of the Fe/silica/Mo(112) system taken at two different bias voltages (10 × 10 nm²). (b) Bias dependence of the apparent height measured for an interfacial Fe^x atom and a dimer.
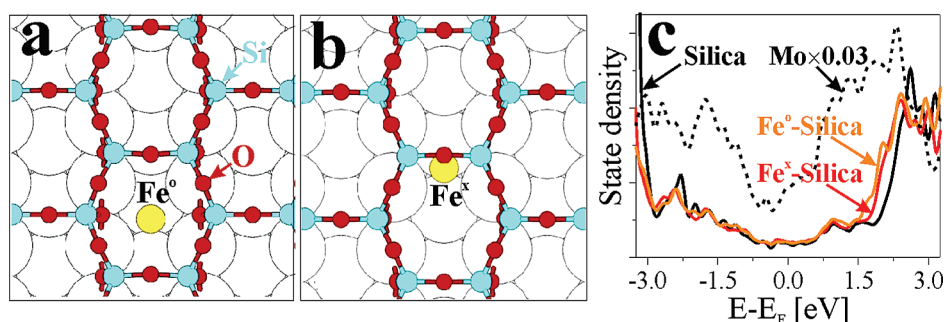
Figure 3. Structure model for Fe atoms in two different binding sites at the silica/Mo(112) interface, (a) below a silica ring and (b) below a [$\bar{1}$10]-oriented Si−O−Si bridge. (c) Calculated LDOS of silica/Mo(112) before (black curve) and after Fe incorporation (red and orange curves). The down-scaled Mo LDOS is depicted by the dashed line.

Mo−Mo bridge positions at the silica/Mo interface are identified as Fe adsorption sites, one being located directly below a silica ring (E_B = 3.3 eV), the other below a [$\bar{1}$10]-oriented Si−O−Si bridge (E_B = 3.6 eV) (Figure 3). In the first configuration, the 4s-orbital of the Fe atom hybridizes with the Si and O atoms of the oxide ring above, resulting in a local increase of the unoccupied state density (LDOS) at the surface (Figure 3c). This particular silica ring now appears brighter than neighboring ones, a situation that is perfectly met by the ring-shaped Fe^o species in Figure 1b. In the second case, the Fe 4s hybridizes only with the Si−O−Si bridge and the LDOS enhancement is confined to a [$\bar{1}$10]-oriented bar in the silica surface. This binding scenario gives rise to the X-shaped contrast of subsurface Fe atoms in the STM. In both adsorption sites, the Fe forms strong covalent bonds with the Mo support and becomes slightly positively charged. The corresponding Bader values are +0.18|e| and +0.03|e| for the Fe^o and Fe^x species, respectively. The binding contribution of the Mo does not affect the STM image contrast, as the Mo−Fe hybrid states are localized at the metal−oxide interface and do not overlap with the tip wave functions.

The intermixing of the Fe 4s orbital and the silica conduction states is also responsible for the apparent height change when imaging the Fe species with increasing sample bias (Figure 2). The calculated Fe-induced state density has a maximum at around 2.1 eV (Figure 3c), and the incorporated Fe indeed appears brightest in STM images taken at 2.5 V (Figure 2b). The small discrepancy between experiment and theory reflects the known deficiency of DFT to reproduce the band gap of insulators. Furthermore, the experimentally observed abundance of Fe^x compared to Fe^o species can be explained by the 10% higher binding energy of the former. The stabilization effect arises from the additional Fe^x interaction with the oxygen ion above and does not occur for the Fe^o species. It is interesting to note that chemically active atoms have, in general, a high tendency to occupy both interfacial binding sites, while the more inert species clearly favor adsorption in the ring positions. Consequently, both X- and ring-

shaped features were observed after exposing the silica film to Li, while only ring-shaped entities appear after Ag and Pd depositon.[11,12,17]

Fe Clusters on the Silica Surface. Larger Fe-related protrusions on the oxide surface, for example, the one shown in Figure 1c, are assigned to Fe adatoms that have attached to a subsurface species.[14] To verify such an anchoring mechanism, the properties of vertical dimers consisting of an interfacial and a surface Fe atom have been explored with DFT. Indeed, both the Fe^x and Fe^o species are able to anchor surface atoms; however, their binding potential differs dramatically. Whereas an Fe^o atom located below a silica ring binds a surface Fe with 1.47 eV, this value drops to 0.24 eV for an Fe^x below a Si−O−Si bridge. The strong binding to Fe^o species is compatible with the short interatomic distance of 2.14 Å. In contrast, Fe surface atoms cannot approach the Fe^x species due to steric repulsion of the silica atoms (d = 3.77 Å), and binding remains weak in this case. The dimer formation is therefore restricted to subsurface species Fe^o atoms, while the Fe^x as the majority species remains monomeric even at high coverage.

According to the DFT calculations, atom attachment to an existing Fe dimer occurs spontaneously and is highly exothermic. Each dimer should therefore constitute the seed for an Fe aggregate, rendering the number of surface clusters identical to the one of subsurface Fe^o species in ring positions. To verify this correlation, samples with increasing Fe content have been prepared and analyzed with the STM (Figure 4). The number of both interfacial Fe species and surface clusters is found to increase linearly with exposure time but maintains a constant ratio of roughly 0.1 (Figure 4d). The absence of saturation effects in the density of incorporated Fe suggests a negligible interplay between incoming atoms and preadsorbed species at the interface in the explored coverage window. Apparently, Fe penetration occurs exclusively at the moment of impact when the atom has sufficient thermal energy to overcome the barrier but not after a finite number of diffusion steps. Those Fe atoms that fail to penetrate the silica top layer become trapped in a physisorption potential of 0.14 eV depth and rapidly diffuse on the ox-
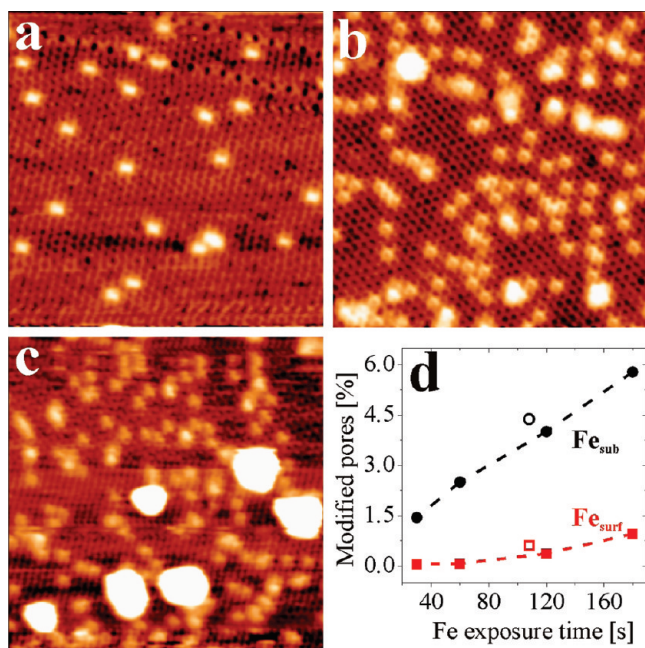
Figure 4. STM images of the silica/Mo(112) film after different Fe exposures (U_s = 0.5 V, 18 × 18 nm²): (a) 20 s, (b) 120 s, and (c) 300 s. (d) Density of subsurface (black) *versus* surface species (red) as a function of the exposure time. The numbers are derived by analyzing STM images as the ones shown in (a−c). Closed and open symbols depict results obtained for Fe deposition at 200 and 300 K, respectively.

ide surface. They are stabilized by attaching either to an Feᵒ species forming a dimer or to a preexisting Fe cluster. The fact that the ratio between subsurface and surface features is similar to the initial Feᵒ to Feˣ ratio corroborates the deceive role of the Feᵒ species in the aggregation process. Surface defects, on the other hand, seem to play only a minor role in cluster formation, reflecting the high structural quality of the silica film.

Additional insight into the Fe penetration behavior through the oxide film is obtained from the ratio between subsurface (n^{sub}) *versus* surface (n^{surf}) Fe atoms. This quantity should follow an Arrhenius behavior as a function of the penetration barrier: $(n^{sub})/(n^{surf}) \propto \exp(-E_{barr}/kT)$ and might be exploited to estimate the barrier height. Whereas n^{sub} is simply determined by counting the monomeric species (Feᵒ and Feˣ) and surface clusters in the STM images, n^{surf} needs to be approximated from the density and height of the Fe clusters, assuming a hemispherical cluster shape and a bulk Fe lattice constant. Analyzing several STM images with different Fe coverage gives a n^{surf} to n^{sub} ratio of approximately 10, manifesting the large number of atoms stored in the surface clusters. Using T = 1100 K for the temperature of the evaporated Fe atoms, the barrier height calculates to 0.23 eV, which is comparable to the DFT value of 0.3 eV. Apparently, the probability to overcome the barrier is mainly determined by the thermal energy of the Fe atoms and not by the substrate temperature. This conclusion is supported by the fact that the ratio between subsurface to surface

species could not be modified by changing the sample temperature during Fe exposure from 300 K to 200 K (Figure 4d, open symbols).

Fe Monomers: Magnetic Properties. After clarifying the morphology of the Fe/silica system, the magnetic properties of the subsurface atoms shall be addressed. A potential use of the Fe atom ensemble as magnetic device requires the conservation of the Fe magnetic moment. Our experimental setup does not permit direct magnetic measurements; however, the mere existence of an Fe spin can be concluded from perturbations of the silica/Mo electronic structure. The underlying physics is captured by the Kondo effect, which describes the formation of a hybrid state between the localized Fe 3d states that carry the magnetic moment and the sp-state continuum of the Mo.[18] The resulting many-body state, referred to as Kondo resonance, screens the Fe magnetic moment by an antiparallel spin alignment of the Mo conduction electrons. The Kondo resonance is located at the Fermi level of the diluted magnetic system and gives rise to distinct Fano-type conductance spectra in the STM.[19,20] The Fano shape hereby originates from quantum interference effects between a direct tunneling path between tip and sample and an indirect one that involves the Kondo resonance. From the width of the Fano line, the Kondo temperature is determined as the critical temperature below which the formation of the many-body electronic state occurs.[8,21,22]

Conductance spectra of both Feᵒ and Feˣ atoms at the silica−Mo interface exhibit indeed a characteristic zero-bias anomaly that is not observed on the pristine film (Figure 5a). This conductance anomaly is spatially localized at the interfacial Fe atoms, as demonstrated with dI/dV maps taken slightly below the Fermi level (Figure 5c). The observed conductance behavior is compatible with the Kondo effect, although other explanations cannot be excluded, such as an Fe-induced change of the single-electron LDOS. Subtraction of a silica background from the Fe spectrum yields a strongly asymmetric line that can be fitted to the Fano model: dI/d$V \propto (q + \varepsilon')^2/(1 + \varepsilon'^2)$ with $\varepsilon' = (\varepsilon - \alpha)/(kT_K)$.[23] Hereby, α denotes the energy position of the Kondo resonance and q is the asymmetry parameter that accounts for the coupling between the localized state and the tip wave function. A satisfactory reproduction of the experimental data is obtained for a Kondo temperature T_K of 122 ± 10 K and a resonance position α of 6 ± 1 mV (Figure 5b). Similar T_K values have been obtained for magnetic adatoms on nonmagnetic substrates, for example, for Co on Ag(111) (92 K)[22] and Au(111) (70 K),[20] supporting the Kondo nature of the observed zero-bias anomaly.[20] However, an unambiguous experimental proof cannot be given at this stage, as this would require conductance measurements performed at different magnetic fields and temperatures.
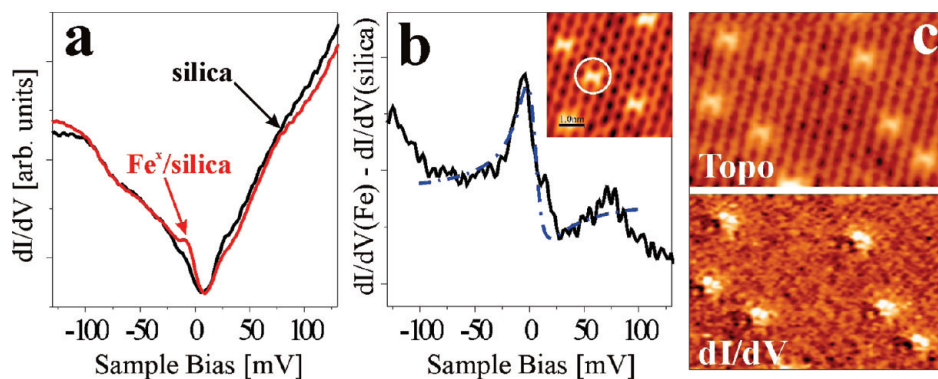
Figure 5. (a) Differential conductance spectra of the bare silica/Mo film (black) and a subsurface Fe^x species (red) (bias set point for spectroscopy: 125 mV). The probed atom is marked by a circle in the inset (5 × 5 nm²). The Fe induces an additional spectral component at the Fermi level. (b) Difference between the Fe^x and the silica/Mo conductance curve. The resulting peak at the Fermi level is fitted with the Fano model (dashed line). (c) Topographic and corresponding conductance image of Fe^x species in the silica/Mo film, taken at a bias position close to the peak maximum in the dI/dV spectrum (U_s = −20 mV, 9 × 6 nm²). The dI/dV map visualizes the strong localization of the conductance anomaly around the embedded Fe atoms.

Also, the DFT calculations are in correspondence with the Kondo scenario, as they obtain a magnetic moment of 1.35 and 2.15 μ_B for the Fe^x and Fe^o species, respectively. Apparently, the magnetic moment of gas-phase Fe atoms (4 μ_B) is reduced but not completely quenched at the silica/Mo interface. Both experiment and theory therefore indicate a magnetic nature of the embedded Fe atoms, which is a crucial requirement for using the porous silica film as a template to fabricate single-atom magnetic units.

CONCLUSIONS

The silica/Mo(112) film is suitable to stabilize monomeric Fe in a two-dimensional array. The atoms penetrate the openings in the silica surface and occupy high-energy binding sites at the metal−oxide interface. In these positions, the Fe atoms are unable to diffuse and agglomerate even at temperatures above 300 K. They are also well-protected against environmental influences due to the inert nature of the oxide layer above. Nonetheless, the magnetic character of the interfacial Fe atoms is preserved. The Fe penetration into the silica pores competes with the formation of few, but large, surface clusters, especially at high Fe exposure. The clusters will produce a spurious signal that interferes with the magnetic response of the atomic entities. However, this undesired effect might be reduced by removing metallic Fe clusters from the surface, for example, by etching, mild sputtering, or ozone treatment. The demonstrated incorporation of Fe into the nanopores of a silica/Mo film is therefore a promising route to fabricate dense ensembles of atom-sized magnetic units for storage devices that do not require operation at cryogenic temperature.

EXPERIMENTAL AND THEORETICAL APPROACH

Experiments were performed with a custom-built STM operated at liquid helium temperature and ultrahigh vacuum conditions. The silica film was prepared by depositing 1.2 ML of silicon in an O_2 ambience of 1 × 10⁻⁷ mbar onto an oxygen precovered Mo(112) surface.[10] Subsequent annealing to 1100 K produced a crystalline oxide film, as proven by a sharp (2 × 2) superstructure pattern in LEED. Iron was evaporated from a high-purity rod and deposited onto the freshly prepared film at 200 K. Spin-polarized DFT calculations were carried out with the generalized gradient approximation as implemented in the VASP code,[24,25] using the PW91 exchange-correlation functional and a plane wave basis set (energy cutoff of 400 eV).[26] The electron−ion interaction was described by the projector augmented wave method.[27] A (4 × 2) super cell consisting of seven Mo layers and the silica film attached to one side was used to model the Fe adsorption behavior (slab stoichiometry $Mo_{56}Si_8O_{20}$). The slabs were separated by 10 Å of vacuum. Except the four bottom Mo layers, all atoms were allowed to relax during geometry optimization until forces dropped below 0.01 eV/Å. Penetration barriers were determined by moving the metal atom along the surface normal into the oxide pore and relaxing the metal/oxide complex for each vertical distance. The computed barrier does not correspond to a real transition state and slightly overestimates the actual barrier height.

REFERENCES AND NOTES

1. Binasch, G.; Grünberg, P.; Saurenbach, F.; Zinn, W. Enhanced Magnetoresistance in Layered Magnetic Structures with Antiferromagnetic Interlayer Exchange. *Phys. Rev. B* **1989**, *39*, 4828–4830.
2. Bansmann, J.; Baker, S. H.; Binns, C.; Blackman, J. A.; Bucher, J.-P.; Dorantes-Dávila, J.; Dupuis, V.; Favre, L.; Kechrakos, D.; Kleibert, A.; *et al.* Magnetic and Structural Properties of Isolated and Assembled Clusters. *Surf. Sci. Rep.* **2005**, *56*, 189–275.
3. Schindler, W.; Hofmann, D.; Kirschner, J. Nanoscale Electrodeposition: A New Route to Magnetic Nanostructures. *J. Appl. Phys.* **2000**, *87*, 7007–7009.
4. Zhang, J.; Repetto, D.; Sessi, V.; Honolka, J.; Enders, A.; Kern, K. Magnetism of Fe Clusters Formed by Buffer-Layer Assisted Growth on Pt(997). *Eur. Phys. J. D* **2007**, *45*, 515–520.
5. Gambardella, P.; Rusponi, S.; Veronese, M.; Dhesi, S.; Grazioli, C.; Dallmeyer, A.; Cabria, I.; Zeller, R.; Dederichs, P. H.; Kern, K.; Carbone, C.; Brune, H. Giant Magnetic Anisotropy of Single Cobalt Atoms and Nanoparticles. *Science* **2003**, *300*, 1130–1133.

6. Heinrich, A. J.; Gupta, J. A.; Lutz, C. P.; Eigler, D. M. Single-Atom Spin-Flip Spectroscopy. *Science* **2004**, *306*, 466–469.

7. Hirjibehedin, C. F.; Lin, Ch.; Otte, A. F.; Ternes, M.; Lutz, Ch. P.; Jones, B. A.; Heinrich, A. J. Large Magnetic Anisotropy of a Single Atomic Spin Embedded in a Surface Molecular Network. *Science* **2007**, *317*, 1199–1203.

8. Zhao, A.; Li, Q.; Chen, L.; Xiang, H.; Wang, W.; Pan, S.; Wang, B.; Xiao, X.; Yang, J.; Hou, J. G.; Zhu, J. G. Controlling the Kondo Effect of an Adsorbed Magnetic Ion through Its Chemical Bonding. *Science* **2005**, *309*, 1542–1544.

9. Gao, L.; Ji, W.; Hu, Y. B.; Cheng, Z. H.; Deng, Z. T.; Liu, Q.; Jiang, N.; Lin, X.; Guo, W.; Du, S. X.; Hofer, W. A.; Xie, X. C.; Gao1, H.-J. Site-Specific Kondo Effect at Ambient Temperatures in Iron-Based Molecules. *Phys. Rev. Lett.* **2007**, *99*, 106402-1–106402-4.

10. Weissenrieder, J.; Kaya, S.; Lu, J. L.; Gao, H.-J.; Shaikhutdinov, S.; Freund, H.-J.; Sierka, M.; Todorova, T. K.; Sauer, J. Atomic Structure of a Thin Silica Film on a Mo(112) Substrate: A Two-Dimensional Network of SiO_4 Tetrahedra. *Phys. Rev. Lett.* **2005**, *95*, 076103-1–076103-4.

11. Ulrich, S.; Nilius, N.; Freund, H.-J.; Martinez, U.; Giordano, L.; Pacchioni, G. Evidence for a Size-Selective Adsorption Mechanism on Oxide Surfaces: Pd and Au Atoms on SiO_2/Mo(112). *ChemPhysChem* **2008**, *9*, 1367–1370.

12. Ulrich, S.; Nilius, N.; Freund, H.-J.; Martinez, U.; Giordano, L.; Pacchioni, G. Realization of an Atomic Sieve: Silica on Mo(112). *Surf. Sci.* **2009**, *603*, 1145–1149.

13. Martinez, U.; Jerratsch, J.-F.; Nilius, N.; Giordano, L.; Pacchioni, G.; Freund, H.-J. Tailoring the Interaction Strength between Gold Particles and Silica Thin Films *via* Work Function Control. *Phys. Rev. Lett.* **2009**, *103*, 056801-1–056801-4.

14. Ulrich, S.; Nilius, N.; Freund, H.-J.; Martinez, U.; Giordano, L.; Pacchioni, G. Modifying the Adsorption Characteristic of Inert Silica Films by Inserting Anchoring Sites. *Phys. Rev. Lett.* **2009**, *102*, 016102-1–016102-4.

15. Giordano, L.; Del Vitto, A.; Pacchioni, G. Au and Pd Atoms Adsorbed on Pure and Ti-Doped SiO_2/Mo(112) Films. *J. Chem. Phys.* **2006**, *124*, 034701-1–034701-7.

16. Giorgi, J. B.; Schröder, T.; Bäumer, M.; Freund, H.-J. Study of CO Adsorption on Crystalline-Silica-Supported Palladium Particles. *Surf. Sci. Lett.* **2002**, *498*, L71–L77.

17. Jerratsch, J.-F.; Nilius, N.; Freund, H.-J.; Martinez, U.; Giordano, L.; Pacchioni, G. Lithium Incorporation into a Silica Thin Film: Scanning Tunneling Microscopy and Density Functional Theory. *Phys. Rev. B* **2009**, *80*, 245423-1–245423-8.

18. Kondo, J. Resistance Minimum in Dilute Magnetic Alloys. *Prog. Theor. Phys.* **1964**, *32*, 37–49.

19. Li, J. T.; Schneider, W. D.; Berndt, R.; Delley, B. Kondo Scattering Observed at a Single Magnetic Impurity. *Phys. Rev. Lett.* **1998**, *80*, 2893–2896.

20. Madhavan, V.; Chen, W.; Jamneala, T.; Crommie, M. F.; Wingreen, N. S. Tunneling into a Single Magnetic Atom: Spectroscopic Evidence of the Kondo Resonance. *Science* **1998**, *280*, 567–569.

21. Madhavan, V.; Chen, W.; Jamneala, T.; Crommie, M. F.; Wingreen, N. S. Local Spectroscopy of a Kondo Impurity: Co on Au(111). *Phys. Rev. B* **2001**, *64*, 165412-1–165412-11.

22. Wahl, P.; Diekhöner, L.; Schneider, M. A.; Vitali, L.; Wittich, G.; Kern, K. Kondo Temperature of Magnetic Impurities at Surfaces. *Phys. Rev. Lett.* **2004**, *93*, 176603-1–176603-4.

23. Fano, U. Effects of Configuration Interaction on Intensities and Phase Shifts. *Phys. Rev.* **1961**, *124*, 1866–1878.

24. Kresse, G.; Hafner, J. *Ab Initio* Molecular Dynamics for Liquid Metals. *Phys. Rev. B* **1993**, *47*, 558–561.

25. Kresse, G.; Furthmüller, J. Efficient Iterative Schemes for *Ab Initio* Total-Energy Calculations Using a Plane-Wave Basis Set. *Phys. Rev. B* **1996**, *54*, 11169–11186.

26. Perdew, J. P.; Chevary, J. A.; Vosko, S. H.; Jackson, A. K.; Pederson, M. R.; Singh, D. J.; Fiolhais, C. Atoms, Molecules, Solids, and Surfaces: Applications of the Generalized Gradient Approximation for Exchange and Correlation. *Phys. Rev. B* **1992**, *46*, 6671–6687.

27. Blöchl, P. E. Projector Augmented-Wave Method. *Phys. Rev. B* **1994**, *50*, 17953–17979.